applied sciences

MDPI

Article

Bulk Grain Cargo Hold Condensation Based on Computational Fluid Dynamics

Honggui Wang * and Hao Zhou

Navigation College, Dalian Maritime University, Dalian 116026, China; zh082021@dlmu.edu.cn
* Correspondence: wanghonggui@dlmu.edu.cn

Abstract: In order to assess whether condensation will occur on the shipside of a bulk grain cargo hold during transportation at sea, this paper has established a ventilation model for the bulk cargo hold of the ship, and optimized the model according to the characteristics of the solid bulk grain stowed on a moving ship at sea. The temperature field, micro-airflow field and relative humidity field of the bulk grain in a cargo hold are simulated by using fluent software (v.2020). Incorporating the impact of grain moisture exchange, the Equilibrium Relative Humidity (ERH) method is introduced alongside the Dew Point (DP) method to determine the condensation on the shipside of the cargo hold. The results of simulation are in agreement with the practical observation results obtained from an actual ship with a heavy cargo damage claim. Conclusively, this paper finds that the risk of the condensation on the shipside of a bulk grain cargo hold always exists if the inner part of the shipside is directly in contact with the grain. Meanwhile, when the grain temperature near the shipside decreases, the moisture in the cargo hold will migrate to the shipside due to the temperature gradient. Furthermore, the longer the voyage, the more obvious the migration of moisture from the central part of the bulk grain to the shipside, and the greater the risk of condensation.

Keywords: cargo hold; temperature and humidity field; condensation; equilibrium moisture; numerical simulation

Citation: Wang, H.; Zhou, H. Bulk Grain Cargo Hold Condensation Based on Computational Fluid Dynamics. *Appl. Sci.* **2023**, *13*, 12878. https://doi.org/10.3390/app132312878

Academic Editor: Jinsong Bao

Received: 22 October 2023
Revised: 26 November 2023
Accepted: 28 November 2023
Published: 30 November 2023

1. Introduction

In recent years, the issue of cargo grain deterioration has received wide attention. Over the past five decades, the grain trade throughout the world has expanded rapidly [1], but almost one-third of the food produced worldwide is lost due to spoilage or waste [2]. According to the classification of the world's major grain trade, soybean accounts for more than 20% [3]. The soybean trade throughout the world is 340.91 million tons in 2020, followed by 324.57 million tons in 2021 and 333.57 million tons in 2022, as shown in Figure 1. From the perspective of transportation mode, shipping is the main means via which the soybean is traded globally. Normally, a single ship can carry approximately 80,000–100,000 tons of soybeans. Once a cargo damage accident occurs, the loss may range from millions to billions (see Table 1).

The storage of bulk grain in a cargo hold of a moving ship, which is very different from the storage of bulk grain on land, is frequently influenced by changing solar radiation and sea temperature. Soybeans are a type of grain sensitive to ambient environmental circumstances [4,5], so when the external temperature decreases, there is a temperature difference between the inside and outside of the grain. The moisture migration, which is caused by temperature gradients, will lead to the creation of high-humidity zones [6] in the hold. The increase in moisture content causes the decomposition of internal substances in soybeans and leads to heat and mold in the grain pile [7–9]. In the process of maritime navigation, the causes of cargo damage accidents include self-heating, mildew, pollution, condensation, wet damage, pests, etc. [10]. Among these factors, condensation is an important factor causing cargo damage. The condensation in a bulk grain hold refers to

the process of water vapor accumulation after the air among the grain particles reaches a saturation state due to a decrease in temperature, as shown in Figure 2. The objective of this paper is to investigate why condensation is produced on the shipside of a cargo hold.

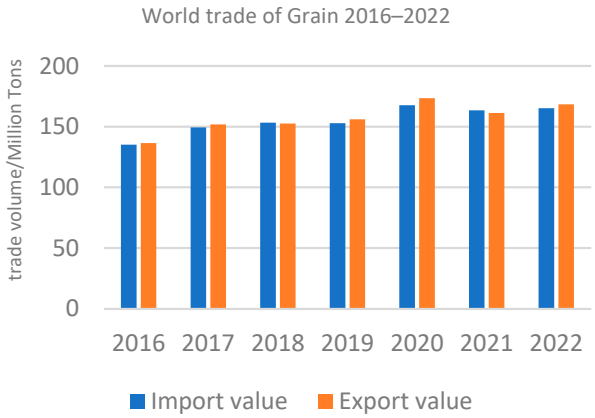

Figure 1. World grain trade during the period from 2016 to 2022.

Table 1. Statistics of damaged bulk grain in tonnage.

No.	Date	Ship Name	Voyage	Damaged Tonnages
(1)	November 1997	MV RAM DAS	India to China	4927
(2)	May 1999	MV Panamax Star	Brazil to China	7001
(3)	April 2004	MV Bunga Saga Lapan	Brazil to China	11,635
(4)	May 2004	MV Hanjin Tacoma	Brazil to China	14,031
(5)	September 2012	MV Tai Prize	Brazil to China	4991
(6)	July 2014	MV Grandamanda	Ukraine to China	20,121
(7)	June 2017	MV Yasa Eagle	Brazil to China	2598
(8)	August 2017	MV ADELANTE	Brazil to China	64,848

Figure 2. Cargo condensation at the stow peripheries.

The problem of the deterioration of bulk grain caused by condensation comes first from the grain storage industry on land. In 1987, Nguyen [11] developed a two dimensional transient model to describe the water transport process due to natural convection within the grain pile, but the model neglected diffusion induced water transport. After this, Kolokotroni et al. [12] experimentally explored moisture distribution in the space

during condensation, and supposed that the vapor distribution is primarily affected by air movement. ABE et al. [13] simulated moisture variations at various locations in 1996 by combining the temperature with the EMC model. In 1998, Chao et al. [14] performed simulations to calculate the effect of thermal buoyancy on air motion. Nine years later, Reed et al. [15] conducted an experimental study of moisture movement and the condensation of grains with high relative moisture content and deterioration. Carrera-Rodriguez et al. [16] conducted numerical simulations of moisture heat transfer in grains with volumetric heat production and the influence of latent heat in 2011. Over the past decade, the research work concerning condensation in bulk grain piles has been conducted to a more detailed degree, and achievement has further increased. In 2021, Kechkin et al. [17] proposed that, when the temperature difference between the grain pile and the external air is between 5 and 6 °C, condensation may occur in the grain pile. In the same year, Yin Jun [18] developed a multi-field coupled mathematical model to simulate the process of grain pile dew condensation changes under a specific temperature difference. More recently, Zhang Ruidi [19] established a condensation experiment simulation platform to explore the occurrence and development of different types of soybean condensation during storage, and found the critical parameters of soybean condensation.

With the increase in bulk grain maritime trade, cargo damage has occurred in the bulk grain cargo hold, and the safe storage of bulk grain during transportation has gradually attracted attention. In 1976, Spencer [20] described the various factors affecting the safe transportation of grain by sea and pointed out that the soybean's own moisture content, breakage, and impurities can affect the grain's safe storage. In 1988, Milton et al. [21] explained the formation of ship sweat and cargo sweat during the transport of grain by ships, reporting that it is the transport of moisture from the inside out that leads to the generation of condensation in the area of contact between liquid water and the cold ship hull. The Transport and Loss Prevention Department of the German Insurance Association [22] reported in 1998 that temperature and moisture content are the two most significant factors affecting the secure transport of soybean by sea, but the degree of influence of each factor was not analyzed in depth. In the 21st century, Palacios [23] examined the temperature and humidity fields of sea-transported coffee seeds, noting that condensation is most likely to occur because of the high humidity in the headspace, and this report offers recommendations for preventing condensation during the transport of coffee beans. In 2018, Drzewieniecka et al. [24] conducted a risk assessment of the soybean meal transport process, observing that the humidity of the ambient air during transport and the size of the bean balancing particles also have a significant impact on the quality characteristics of the cargo. In recent years, Uygun et al. [25] described the risk of transporting cocoa beans by ship in terms of five aspects: humidity, moisture content, condensation, post-fermentation, insect damage and mold, and simulated these with software. In 2020, Anderson et al. [26] explained the properties of the self-nature of different types of grain during maritime transport, and presented the corresponding theoretical basis. In the same year, Lovstad [27] provided evidence of the negative effects of high grain moisture content during ventilation. In 2021, Yuen et al. [28] explored the container condensation mechanism and developed a statistical model to estimate the condensation probability by considering external weather. Subsequently, Tatyana et al. [29] explored the phenomenon of moisture absorption and desorption of hygroscopic goods when transported by sea, and summarized the moisture content range to prevent condensation of cargo. At the same time, Ocieczek et al. [30] conducted an experimental study of the sensitivity of different types of grain to the marine transportation environment, and pointed out that the best grain to prevent condensation is rye. In summary, the research work on safe storage of bulk grain on land is more developed than that onboard ships. Only a few studies have been conducted on the issue of condensation in the ship's cargo. Therefore, this paper has carried out innovative work from the following aspects:

(1) A model is developed after giving consideration to the dynamic fluctuations in sea temperature and sun radiation within the cargo hold;

(2) The condensation of grain near the side of the cargo hold is explored;
(3) The risk of grain particle surface condensation within the cargo hold has been verified by actual ship data and mathematical equations.

2. Mathematical Model

2.1. Traditional CFD Fluid Equations

In this analysis, it is assumed that:

(1) The airflow in the cavity is incompressible Laminar Flow;
(2) In addition to the density in the buoyancy term in the momentum equation, the thermophysical properties of the fluid are assumed to be constant;
(3) The moisture-absorbing porous media is considered to be bulk wheat, which is uniform, isotropic, and in local thermodynamic equilibrium with the surrounding air.

The law of conservation of mass is expressed by:

$$\frac{\partial \rho}{\partial t} + \nabla \cdot (\rho u_{\mathrm{i}}) = 0 \tag{1}$$

where ∇ is the Hamiltonian; u_{i} (i = i, j, k) is the airflow velocity of air, m/s; t is time, s; and ρ is the fluid density, kg/m^3.

The law of conservation of momentum is expressed by:

For the consideration of natural convention in the grain pile and the simplification of the calculation, the Boussinesq Equation is expressed as follows [31]:

$$\rho \frac{\partial u_{\mathrm{i}}}{\partial t} = -\frac{\partial P}{\partial x_{\mathrm{i}}} + \delta_{\mathrm{ij}} \rho_0 g[1 - \beta(T - T_0)] - \frac{\varphi \mu u_{\mathrm{i}}}{K} \tag{2}$$

where p is the static pressure of air, Pa; g is the gravitational acceleration, m/s^2; μ is the dynamic viscosity of the fluid, Pa·s; T_0 and T are the initial and real-time temperatures of the grain pile, K; ρ_0 is the density of air at temperature T_0; φ is the equivalent diameter of grain particles, mm; β is the volume expansion coefficient of air; and K is the permeability of the grain pile.

The law of conservation of energy is expressed by:

$$\frac{\partial T}{\partial t}(\rho_{\mathrm{s}} C_{\mathrm{s}}) + C\nabla \cdot (\rho v T) = k_{\mathrm{eff}} \nabla^2 T + S_{\mathrm{h}} \tag{3}$$

where ρ_{s} is the density of soybean, kg/m^3; C_{s} is the specific heat capacity of soybean, J/(kg·K); C is the specific heat capacity of air, J/(kg·K); k_{eff} is the effective heat transfer coefficient of soybean, W/(m·K); and S_{h} is the source term, which includes the heat generated by grain respiration [32] and the heat of moisture absorption or desorption:

$$S_{\mathrm{h}} = \rho_{\mathrm{s}} q_{\mathrm{h}} Y_{\mathrm{co_2}} + h_{\mathrm{s}}(1 - \varepsilon)\rho_{\mathrm{s}} \frac{\partial W_{\mathrm{g}}}{\partial t} \tag{4}$$

where q_{h} is the heat release from the respiration process with a value of 10.738 J/mg; and Y_{CO2} is the CO_2 release rate of the grain pile respiration for 24 h, mg/kg. The following equation is shown [33]:

$$\log_{10}(Y_{co_2}) = -4.054 + 0.0406(T) - 0.0165(\theta) + 0.0001(\theta)^2 + 0.2389(W_{\mathrm{g}}) \tag{5}$$

where T is the temperature, °C; θ is the storage date, d; and W_{g} is the grain moisture content.

2.2. Optimization of the Traditional CFD Fluid Equations

2.2.1. Application of Solar Radiation Model

During the transportation of bulk grain at sea, solar radiation directly affects the temperature of a bulk cargo by the irradiating hatch cover. Therefore, the solar tracing algorithm is chosen to load the solar model into the mathematical model. Meanwhile, there

is a radiation heat exchange between the structure, so the radiation heat transfer process could be considered in the numerical calculation. The Discrete Ordinates (DO) radiation model can be opaque or semi-transparent to the material. This radiation model is chosen to solve the solar radiation and heat exchange in the ship's cargo hold. The specific equations are given in the following equation [34]:

$$\nabla \cdot (I(\boldsymbol{r},\boldsymbol{s})\boldsymbol{s}) + (\alpha + \sigma_s) \cdot I(\boldsymbol{r},\boldsymbol{s}) = \alpha \cdot n^2 \cdot \frac{\sigma \cdot T^4}{\pi} + \frac{\sigma_s}{4\pi}\int_0^{4\pi} I(\boldsymbol{r},\boldsymbol{s}) \cdot \Phi(\boldsymbol{s},\boldsymbol{s}') \cdot \mathrm{d}Q' \quad (6)$$

where r is the position vector of radiation transfer; s is the direction vector of radiation transfer; s' is the scattering direction vector of radiation; α is the absorption coefficient of shipside; n is the refraction coefficient of shipside; σ_s is the scattering coefficient of shipside; σ is the Stephen Boltzmann constant, which takes the value of 5.672×10^{-8} W/(m^2·K^4); I is the radiation intensity, W/m^2; Φ is the phase function; and Ω' is the stereo angle of radiation, $180^2/\pi^2$.

2.2.2. Application of Sea Temperature Change

The change of sea temperature is another important factor affecting the shipside environment. In contrast to land-based silos, ships typically traverse vast latitudes, leading to significant fluctuations in sea temperature and substantial temperature differentials. In this paper, the sea temperature is intercepted from the historical chart data and drawn into a curve, as shown in Figure 3, and the data are imported into the software.

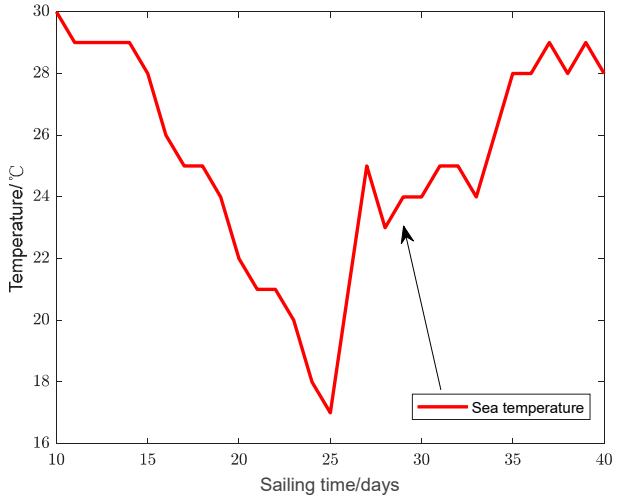

Figure 3. Sea temperature variation through ship navigation.

2.2.3. Application of Moisture Conservation Equation

According to the moisture content of soybean and the absolute moisture content in the air between soybeans during convective diffusion, satisfying the conservation law [31,35], the moisture equation is added to quantify the risk of condensation:

$$\frac{\partial(\varepsilon\rho\omega)}{\partial t} + \nabla \cdot (\rho u\omega) = \nabla \cdot (\rho D_{\mathrm{eff}} \nabla\omega) - (1-\varepsilon)\rho_s \frac{\partial W_g}{\partial t} + \rho_s q_W Y_{CO_2} \quad (7)$$

where ω is the absolute moisture content of the air between the particles, kg/kg; D_{eff} is the effective diffusion coefficient of water vapor, m^2/s; and q_w is the amount of water produced by the respiration process, which is 4.09×10^{-5} kg /mg [36].

2.2.4. Calculation of Relative Humidity Inside Grain Bulk

In the simulation and measurement, it is necessary to convert the moisture content and related data from the formula to relative humidity for comparison, as shown in the following formula [37]:

$$RH = 10 \times (101.325 \times \omega)/(0.621945 + \omega) \times 1.0016 + 3.15 \times 10^{-6} \times p - 0.074 \times p^{-1} \times 6.112 \times \exp(17.67 \times (T - 273.15)/(T - 29.65) \times 1.0016 + 3.15 \times 10^{-6} \times p - 0.074 \times p^{-1}) \quad (8)$$

where RH is the relative humidity of bulk grain, T is the temperature, K; and P is the fluid pressure, kPa.

When the moisture content is unknown and the dew point temperature and grain temperature are known, the relative humidity can be calculated based on the Magnus-Tetens Approximation [38]:

$$RH = \exp(17.27 \times DP/(237.7 + DP) - 17.27 \times T/(237.7 + T)) \quad (9)$$

where T is the temperature, °C; and DP is the dew point temperature, °C.

2.3. Determination of Vapor Condensation on the Shipside of a Cargo Hold

2.3.1. DP Method

During ship navigation, the water vapor content in the air remains constant if a cargo hold is taken as a whole unit and is not ventilated during transportation at sea. Due to the impact of the navigation environment, the temperature of some interior areas will drop, and correspondingly the relative humidity in these areas will progressively rise. When the temperature reaches a specific point, the vapor in the air approaches a saturation state. At this time, if there is a further drop in ambient temperature, condensation of supersaturated water vapor begins to appear. The temperature at this time is referred to as the DP temperature. To assess if there is a risk of condensation developing in the bulk cargo hold throughout the navigation, the DP method is used in this study by comparing the temperature of the cargo hold and the dew temperature.

2.3.2. ERH Method

The ERH refers to the level of humidity present in the grain at which the water vapor pressure in both the grain and the surrounding atmosphere are in a state of equilibrium. When the ambient humidity is higher than the grain equilibrium humidity during transport, grain and atmosphere are in the process of humidity exchange, which results in a tendency towards grain particle surface condensation. Therefore, to better determine the condensation risk of grain, the ERH method [39] is employed, with the formula as follows:

$$ERH = \exp\left\{\frac{\frac{D}{222} \times \left(e^{\frac{5.795 - W_g}{2.886}} - e^{\frac{1.104 - W_g}{4.114}}\right) \times \left(1737.1 - \frac{474242}{273 + t}\right) + 192.109 \times \left(1 - e^{\frac{5.795 - W_g}{2.886}}\right) + 202}{87.72}\right\} \quad (10)$$

where ERH is the grain ERH; and T is the grain temperature, °C.

3. Numerical Simulation

3.1. Ship Cargo Hold Parameters

M/V Bakebolan was selected for analysis of the effects produced by condensation inside the cargo hold. The ship departed from Brazil on 2 July 2019, through the Mediterranean Sea and the Gulf of Aden, and then went north through the Strait of Malacca to reach the Longkou port, China, 43 days later. The route is shown with the red line in Figure 4. According to the ventilation records, the ship was surface ventilated. In this paper, the fourth cargo hold of the ship was modeled to simulate the temperature and humidity fields in the ship's cargo hold during the arrival at Longkou. The cargo hold parameters are shown in Table 2.

Figure 4. Navigation route of M/V Bakebolan from Brazil to China.

Table 2. Cargo hold particulars.

Parameters	Value
Ship Summer Displacement	82,150 T
The Cargo loaded	69,699 T
Ship voyage draft	11.1 m
Cargo hold length	32.2 m
Cargo hold width	28.6 m
Cargo hold depth	17.5 m

3.2. Grid Division

In this paper, the ship 's topside tank, hopper tank and bottom shell plating are not modeled; their effects on the cargo hold have been incorporated by changing the convective heat transfer coefficient, and the convective heat transfer coefficient is obtained according to the method in reference [40].

The cargo hold is meshed by the Multizone method, with various mesh densities selected for the lower soybean storage area and the air area at the top of the cargo hold, and the overall structured hexahedral mesh is employed. For improvement in the accuracy of the numerical simulation's calculation results, the grid of the boundary layer is encrypted based on the curvature and narrow slit functions, and then generated 300 thousand grids. Figure 5 illustrates the cargo model and mesh division. After grid independence verification, the simulation results of this study are shown to be accurate and reliable, and meet the calculation accuracy requirements.

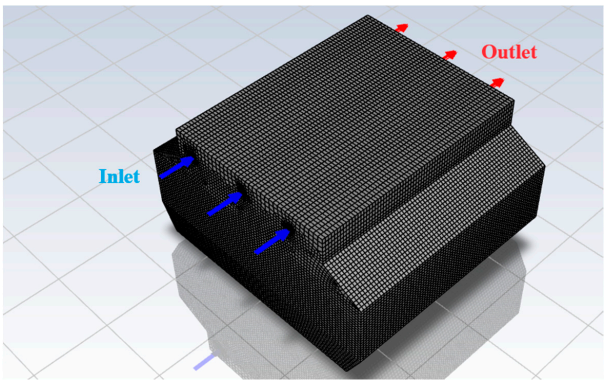

Figure 5. Grid division of ship cargo hold.

3.3. Initial Simulation Parameter Setting

3.3.1. Initial Conditions

The density of the bulk soybean grain pile was set to 769.7 kg/m^3, the specific heat capacity of the pile was set to 1870 kJ/(kg·K), and the thermal conductivity of the pile was set to 0.13 W/(m·K). The bulk soybean was modeled as an isotropic porous medium with a porosity of 0.5.

3.3.2. Boundary Condition

(1) Solar Radiation Boundary

For the solar radiation during the ship's voyage, because the radiation to the hatch enclosure at the hatch is only present in the morning and evening, the angle of incidence of the sun on the hatch coaming is small, so the radiation of the sun on the hatch coaming is also small. Therefore, to shorten the calculation time and improve the accuracy of the calculation results, assuming that solar radiation only affects the hatch enclosure during ship navigation, the absorption coefficient of the cargo hold hatch cover is set to 0.8.

(2) Sea Convective Heat Exchange Boundary

1. The shipside and the bottom of the cargo hold are set as the convective wall. The heat transfer coefficient of the wall in contact with seawater is set to 7616.36 W/m^2·K [40] and the heat transfer coefficient of the wall in contact with air is set to 5.62 W/m^2·K.

(3) Ventilation Boundary

2. According to the ventilation record, the ventilation time from 2 July to 16 August is shown in Table 3.

Table 3. Ventilation recording data during the period from July 2 to August 16.

Date	Ventilation	Ventilation Record
2 July–12 July	No	Fumigation
13 July–19 July	Yes	Ventilation
20 July–25 July	No	Wind and waves
26 July–7 August	Yes	Ventilation
8 August	No	Rainfall
9 August–16 August	Yes	Ventilation

The voyage started on 2 July 2019, and the navigation to Longkou was completed on 16 August 2019. Since the ventilation form was natural ventilation with small speed, the air inlet wind speed was set to 1 m/s, and the outlet was set to pressure outlet according to the feedback data from the ship. In this paper, it is assumed that the grain surface is fully ventilated.

In summary, the simulation boundary conditions for the ship's cargo hold storage and transportation process are set as in Table 4:

Table 4. Setting of boundary conditions and parameters.

Name	Boundary Type	Parameter	Value
Ventilation inlet	Speed Inlet	Wind velocity, v_{in}	1 m/s
Ventilation outlet	Pressure outlet	Gauge pressure,P_{out}	0 Pa
Grain	Porous media	Soybean density, ρ_g	769.7 kg/m^3
		Specific heat capacity, C_g	1870 kJ/(kg·K)
		Thermal conductivity, λ_g	0.13 W/(m·K)
		Porosity, φ	0.5
		Viscosity coefficient, γ	1.2×10^9 m^2/s
		Inertial resistance, C_2	2800

Table 4. *Cont.*

Name	Boundary Type	Parameter	Value
Convection wall	Boundary	Convection heat transfer coefficient, h	7616.36 W/(m^2·K)
		Steel density, ρ_s	8030 kg/m^3
		Conductivity coefficient, λ_s	16.27 W/(m·K)
		Specific heat, C_s	502.48 J/(kg·K)
Radiant Wall	Boundary	Absorption,α	0.8

3.3.3. Simulation Process

In summary, the research framework of this article is shown in Figure 6. Firstly, the basic physical model is established, and then the model is optimized and improved according to the particularity of the bulk grain cargo hold. The moisture equation and the heat source term are incorporated into the model in order to simulated the dynamic changes in humidity and temperature within the cargo hold, and the alterations in sea temperature and solar radiation are incorporated into the establishment of boundary conditions.

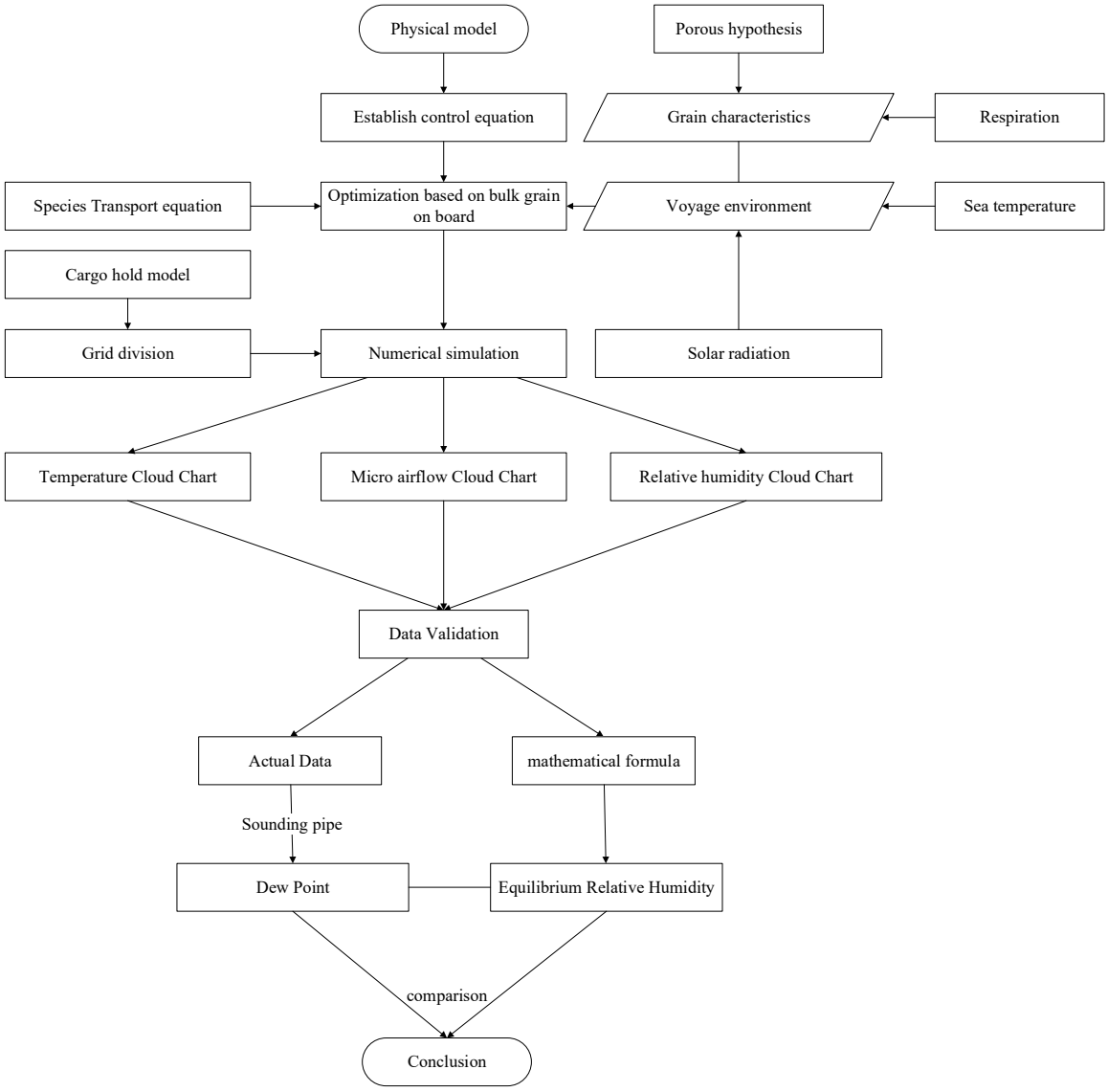

Figure 6. Research Framework.

Secondly, the temperature, micro-airflow, and humidity data collected during the ship's navigation are computed and later transmitted to the contour. In addition, a comparative analysis is conducted comparing the temperature data and the recorded DP data aboard the ship. Similarly, the humidity data is contrasted with the ERH to arrive at a conclusive inference.

3.4. Results and Analyses

The temperature and humidity contours were obtained from 13 July to 16 August. The temperature, micro-airflow field, and moisture distribution of the cargo hold on 23 July, 3 August, and 13 August were selected, as shown in Figures 7–9.

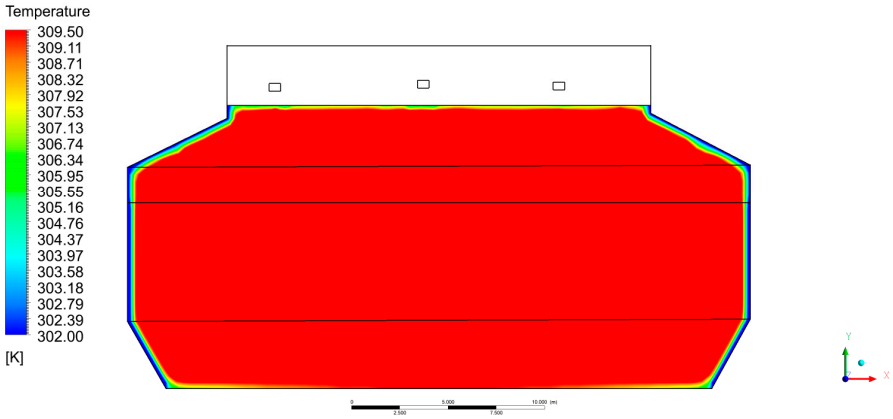

Figure 7. Contour of cargo hold ventilation temperature field on 23 August 2019.

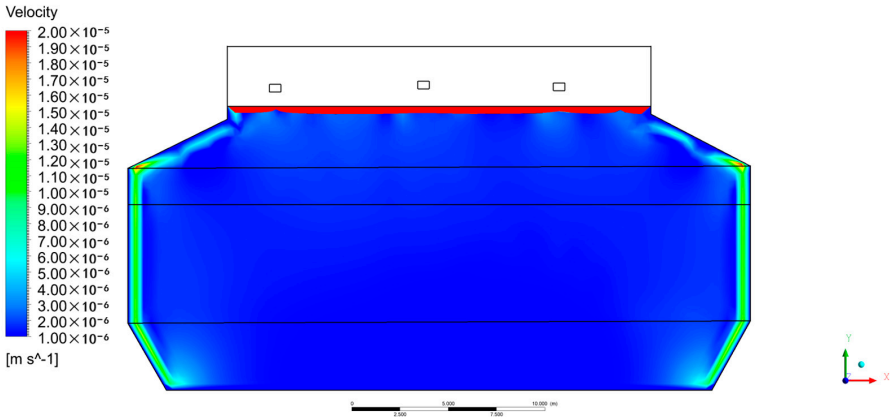

Figure 8. Contour of cargo hold micro-airflow field on 23 August 2019.

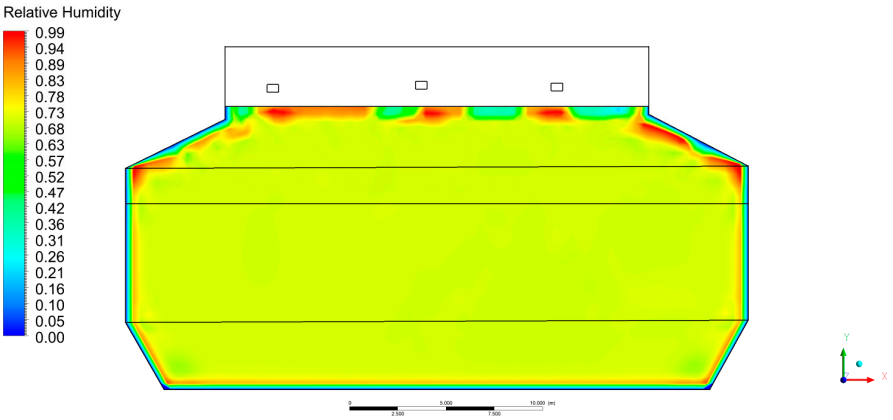

Figure 9. Contour of cargo hold relative humidity field on 23 August 2019.

3.4.1. Soybean Temperature Field Simulation

As can be seen from Figure 7, in the case of the same initial temperature inside the cargo hold, the temperature of soybean in different locations gradually produces large differences; the temperature at the side gradually decreases due to the influence of convective heat transfer from the sea, and this affects the soybean close to the side. With the increase in navigation time, the low-temperature area gradually spreads inward. Due to the impact of ventilation, the temperature of the surface layer of soybean is reduced; and the soybean internal respiratory exotherm, due to the grain, results in a gradual increase in internal temperature.

3.4.2. Soybean Micro-airflow Field Simulation

As can be seen from Figure 8, the micro-airflow in the soybean pores is mainly driven by the temperature gradient with a slow velocity, and the order of magnitude mainly resides at 10^{-6} m/s. It is obvious that the micro-airflow velocity at the shipside is higher in comparison to velocities observed at other positions. The micro-airflow inside the grain shows a closed trend, from the internal "hot core" from the bottom up to near the surface of the grain, then through the convection low-temperature wall from top to bottom, and finally through the bottom of the grain back to the center, which is counterclockwise. Due to the influence of self-heating on the internal temperature of soybean and convective heat transfer on the side, the temperature gradient gradually increases with the increase in navigation time, and the micro-airflow velocity is on the rise, reaching a maximum of 1×10^{-5} m/s, which also indicates that the natural convective flow of air inside the grain pile is Laminar Flow. The above analysis results are consistent with the description in the literature [18,41].

3.4.3. Soybean Relative Humidity Field Simulation

From Figure 9, the change in soybean humidity field varies with the change in temperature field and micro-airflow field. The relative humidity is high in the cargo near the shipside, and the relative humidity inside the grain decreases as the temperature rises. With the increase in transport time, the moisture content on the shipside is increasingly elevated. This is consistent with the principle of negative correlation between temperature and moisture in the stability of grain storage. The reason is that the temperature inside the grain is increased by respiration, and the temperature near the side is decreased by sea convection, resulting in a temperature difference between the inside and outside of the grain. Due to the proportional relationship between vapor pressure and temperature, the temperature difference leads to the generation of internal and external pressure differences. To balance the pressure difference, water vapor is transported from inside to outside, resulting in the generation of a high humidity area on the shipside. This area is prone to condensation, coupled with the influence of cold air on the low-temperature wall of the side.

3.5. Verification

Via the DP method and ERH method, the risk of condensation on the shipside of the cargo hold is verified.

3.5.1. The Verification by Actual Data

For detecting the temperature and the DP temperature, modern solid bulk ships are installed with one or two sounding pipes in each cargo hold [42]. The sounding pipe is normally located near the centerline of the ship before or after a hold, if only one sounding pipe is installed. The sounding pipes are located near both sides, if two are installed. In the ship engaged in this study, two sounding pipes are installed in each hold. The location of the sounding pipes of No.6 cargo hold is shown in Figure 10. The left pipe is used for a sinkhole, and the right pipe is the sounding pipe. From the diagram, it can be seen that the sounding pipe is close to the shipside position, hence this research can chooses the measured data to represent the temperature and the DP temperature data on the shipside.

(**a**) (**b**)

Figure 10. No.6 cargo hold sounding pipe. (**a**) Sounding pipe deck part; (**b**) Sounding pipe bottom part.

When the crew measured the cargo temperature and DP temperature inside the cargo hold by using the sounding pipe, the appropriate length of the line was connected to the plug at the top of the sounding pipe, and the dry and wet bulb thermometer was hung in the sounding pipe, which could be extended to the bottom. After each ventilation, the ship's crew placed the wet and dry bulb thermometer in the sounding pipe and, waiting about one hour to allow enough air to flow through the wet bulb to evaporate, and then removed the thermometer to record the temperature and DP temperature data.

In this paper, the closest point to the bottom of the sounding pipe is selected in the model to compare with the actual ship data. Based on the findings presented in Figure 11, it can be observed that the difference between the simulation data and the actual ship data is below 5%, With the increase in navigation time, the difference between the simulated temperature and the measured temperature gradually decreases, and the minimum is 0.3 °C, while the difference between the simulated relative humidity and the measured relative humidity fluctuates at 4%. Simultaneously, it has been observed that alterations in temperature and humidity at the shipside are mostly influenced by fluctuation in sea temperature. However, it should be noted that the cargo hold environment discussed in this study is based on ideal conditions. In reality, the alteration of actual ship data is a more intricate process compared to the simulation data. However, over the entirety of the modeling phase, the observed fluctuations in average temperature and humidity of soybean closely align with those seen in actual ship conditions.

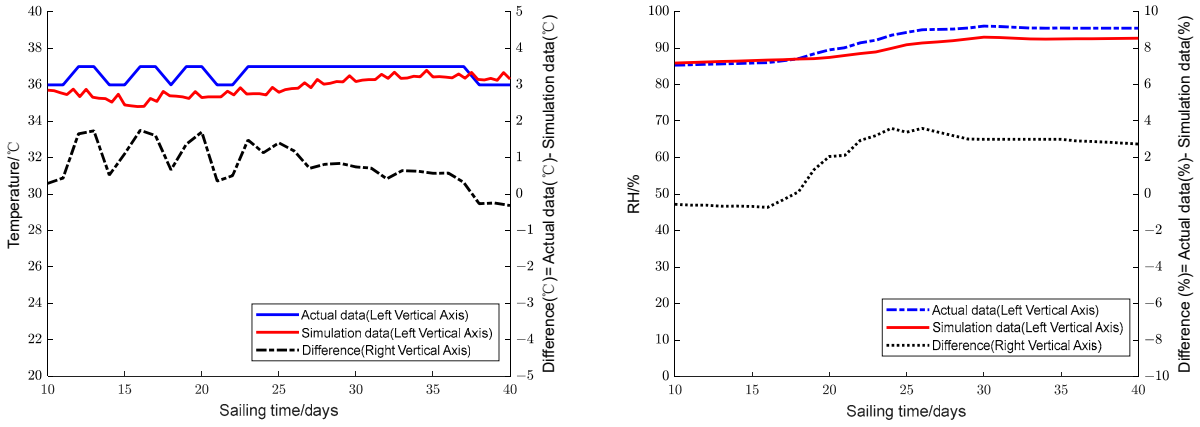

(**a**) (**b**)

Figure 11. Temperature and humidity contrast shipside. (**a**) Temperature contrast of shipside; (**b**) Humidity contrast of shipside.

3.5.2. Verification by DP Method

As shown in Figure 12, with the increase in navigation time, the fluctuation in soybean temperature and DP temperature in the cargo hold near the shipside is intensified, which is caused by the frequent change in sea temperature. The data obtained from the simulation and monitoring of the cargo hold indicates that the temperature of the soybean near the shipside always approaches the DP temperature. After a period of time, with the decrease in the side temperature and the increase in the moisture content, the difference between the temperature and the dew point temperature tends to decrease, and the largest disparity between these temperatures is only 2 °C, which means the DP temperature can be easily reached. This observation confirms that the shipside is susceptible to the risk of dew condensation due to the micro-airflow driven by the temperature gradient.

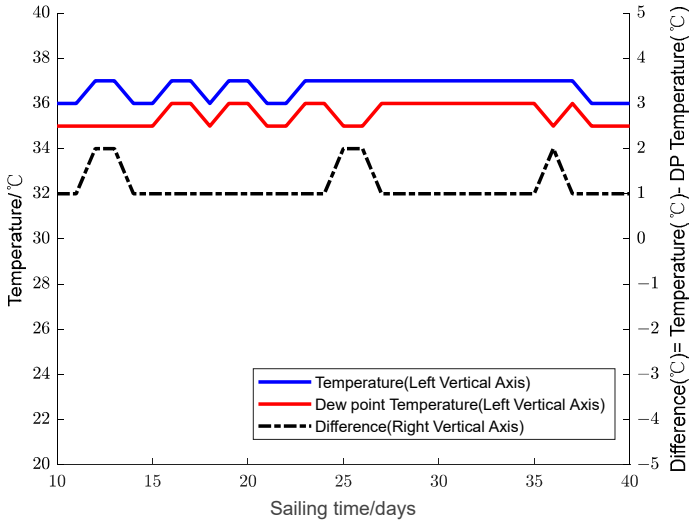

Figure 12. DP temperature contrast shipside.

3.5.3. Verification by ERH Method

The curve of the ERH of the grain in the hold during the ship's voyage since July 13 is calculated according to Equation (9); the actual relative humidity is used to compare with the ERH, and analyzed by calculating the difference.

From Figure 13, it can be observed that the fluctuation in temperature and humidity in the cargo hold leads to varying levels of relative humidity and ERH. After the ship finished fumigation, the shipside of the cargo hold presented a rise in humidity level, which reached a value of 85.31% on the 10th day. Throughout the early stage of the navigation, the sea temperature consistently decreased, resulting in a lower temperature of soybean near the shipside compared to its interior temperature. Consequently, there was a persistent outward diffusion of moisture, then relative humidity at the shipside shows an upward trend. On the 18th day of navigation, the relative humidity reached 87.32%, surpassing the ERH, and the soybean exhibited an unstable condition. During the latter stage of the navigation route, there was an increase in sea temperature, the temperature difference between inside and outside of the cargo hold is reduced, and the rising trend in relative humidity decreased. Comparing the difference value, it can be seen that the maximum difference reaches 8%. The difference value substantiates the presence of a potential condensation risk at the shipside of the cargo hold.

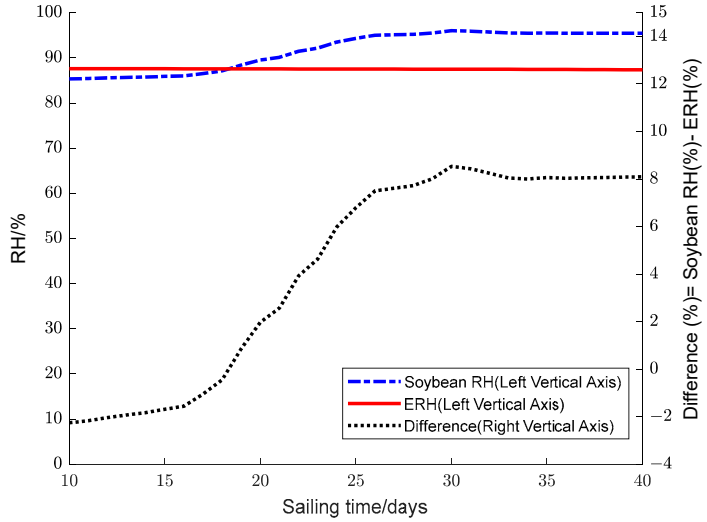

Figure 13. Relative humidity contrast shipside.

4. Discussion

From the result, it can be determined that the cargo hold side temperature is the main cause of condensation, while the higher convective heat transfer coefficient of the bulkhead and the variable sea temperature are the central factors. Unlike other cargoes, matting material cannot be used to prevent contact with the cargo hold, but when we put about 0.5 cm of thermal insulation coating on the bulkhead of the cargo hold, the thermal conductivity of the thermal insulation coating was just 0.05 $W \cdot m^{-1} \cdot K^{-1}$ [43], so it is capable of efficiently reducing the effect of the sea temperature from the shipside of the cargo hold to almost zero. By reducing the temperature difference inside the cargo hold, it might effectively prevent the condensation caused by the outward transport of moisture in the cargo hold. However, for the analysis of the cargo, if the moisture content of soybeans exceeds 12.5%, both the real-time temperature and the current relative humidity in the cargo hold are close to the critical value, and there is already a risk of condensation, so it is advisable to ensure that the initial moisture content of soybean does not exceed 12.5% prior to the start of the voyage.

5. Conclusions

CFD technology is used to simulate the environment in the cargo hold of a ship storing soybean, the temperature and humidity as well as the micro-airflow contour charts in the cargo hold are obtained, and the following conclusions can be obtained by comparison with the actual data:

(1) In the voyage selected in this paper, the temperature of soybean in the deep part of the cargo hold exceeds 35 °C, which is a high temperature grain storage state. This occurrence is attributed to the combined influence of sea temperature, sun radiation, and grain respiration. Under the action of micro-airflow, the moisture inside the grain migrates outward, and the relative humidity of the grain at the shipside reaches 95%.

(2) The simulation demonstrates a correlation between the production of micro-airflow and the temperature gradient within the grain bulk. Additionally, the temperature and micro-airflow exhibit a coupling effect on the distribution and alteration of relative humidity inside the grain bulk.

(3) With the increase in navigation time, the moisture is continuously transported from the inside to the outside of the cargo hold, and the temperature of the shipside of the cargo hold is continuously reduced, so the risk of condensation is greater.

The quality safety of grain on board is a complex issue, involving many factors, such as the quality of the grain, the ship's transportation time, the average moisture content of the grain, the degree of moisture homogenization of the grain, the temperature and humidity

at the time of loading, the grain size, the impurity content, the broken seed content, the oil content of the grain, the temperature gradient of the sea area sailed through, the solar radiation intensity, the surface ventilation, etc. This paper only verifies the risk of dew condensation in the shipside position by CFD simulation and through the ship, and other related issues deserve further study.

Author Contributions: Conceptualization, H.W. and H.Z.; methodology, H.Z.; software, H.Z.; validation, H.W.; formal analysis, H.Z.; investigation, H.W.; resources, H.W.; data curation, H.Z.; writing—original draft preparation, H.Z.; writing—review and editing, H.W.; visualization, H.Z.; supervision, H.W.; project administration, H.W.; funding acquisition, H.W. All authors have read and agreed to the published version of the manuscript.

Funding: The work presented in this paper was financially supported by the National Natural Science Foundation of China (Grant No. 52101399).

Institutional Review Board Statement: Not applicable.

Informed Consent Statement: Not applicable.

Data Availability Statement: All data, models, or code that support the findings of this study are available from the corresponding author upon reasonable request. The data are not publicly available due to privacy restrictions.

Conflicts of Interest: The authors declare no conflict of interest.

References

1. Liu, F. Analysis of Soybean International Trade Network. Master's Thesis, Beijing Institute of Technology, Beijing, China, 2016.
2. Jian, F. A general model to predict germination and safe storage time of crop seeds. *J. Stored Prod. Res.* **2022**, *99*, 102041. [CrossRef]
3. Coradi, P.C.; Lima, R.E.; Padia, C.L.; Alves, C.Z.; Teodoro, P.E.; Carina da Silva Cândido, A. Soybean seed storage: Packaging technologies and conditions of storage environments. *J. Stored Prod. Res.* **2020**, *89*, 101709. [CrossRef]
4. Crops and Livestock Products. Available online: https://www.fao.org/faostat/en/#data/TCL (accessed on 30 August 2023).
5. Capilheira, A.; Cavalcante, J.; Gadotti, G.I.; Bezerra, B.; Hornke, N.; Villela, F. Storage of soybean seeds: Packaging and modied atmosphere technology. *Rev. Bras. De Eng. Agrícola E Ambient.* **2019**, *23*, 883. [CrossRef]
6. Mohos, F. Water Activity, Shelf Life and Storage. In *Confectionery and Chocolate Engineering*; John Wiley & Sons, Inc.: Hoboken, NJ, USA, 2017; pp. 579–603.
7. Coradi, P.C.; Souza, A.; Camilo, L.; Lemes, Â.; Milane, L. Analysis of the physical quality of genetically modified and conventional maize grains in the drying and wetting processes. *Rev. Ciência Agronômica* **2019**, *50*, 370–377. [CrossRef]
8. Magan, N.; Lacey, J. Effects of gas composition and water activity on growth of field and storage fungi and their interactions. *Trans. Br. Mycol. Soc.* **1984**, *82*, 305–314. [CrossRef]
9. Fleurat-Lessard, F. Qualitative reasoning and integrated management of the quality of stored grain: A promising new approach. *J. Stored Prod. Res.* **2002**, *38*, 191–218. [CrossRef]
10. Woerfel, J.B. Chapter 4—Harvest, Storage, Handling, and Trading of Soybeans. In *Practical Handbook of Soybean Processing and Utilization*; Erickson, D.R., Ed.; AOCS Press: Urbana, IL, USA, 1995; pp. 39–55.
11. Nguyen, T.V. Natural Convection Effects In Stored Grains—A Simulation Study. *Dry. Technol.* **1987**, *5*, 541–560. [CrossRef]
12. Kolokotroni, M.; Saiz, N.; Littler, J. Moisture movement: A study using tracer gas techniques and CFD modelling. *Build. Serv. Eng. Res. Technol.* **1992**, *13*, 113–117. [CrossRef]
13. Abe, T.; Basunia, M.A. Simulation of Temperature and Moisture Changes During Storage of Rough Rice in Cylindrical Bins Owing to Weather Variability. *J. Agric. Eng. Res.* **1996**, *65*, 223–233. [CrossRef]
14. Chao, N.-T.; Wang, W.-A.; Chiang, C.-M. A study of a control strategy utilizing outdoor air to reduce the wintertime carbon dioxide levels in a typical Taiwanese bedroom. *Energy Build.* **1998**, *29*, 93–105. [CrossRef]
15. Reed, C.; Doyungan, S.; Ioerger, B.; Getchell, A. Response of storage molds to different initial moisture contents of maize (corn) stored at 25 °C, and effect on respiration rate and nutrient composition. *J. Stored Prod. Res.* **2007**, *43*, 443–458. [CrossRef]
16. Carrera-Rodríguez, M.; Martínez-González, G.M.; Navarrete-Bolaños, J.L.; Botello-Álvarez, J.E.; Rico-Martínez, R.; Jiménez-Islas, H. Transient numerical study of the effect of ambient temperature on 2-D cereal grain storage in cylindrical silos. *J. Stored Prod. Res.* **2011**, *47*, 106–122. [CrossRef]
17. Kechkin, I.; Ermolaev, V.; Belyaeva, M.; Tarakanova, V.; Gurkovskaya, E.; Buzetti, K. Processes of Heat and Mass Transfer During Grain Mass Storage in Metal Silos of Large Capacity. *KnE Life Sci.* **2021**, *6*, 206–214. [CrossRef]
18. Yin, J. Research on Multi-Fields Coupling Model of Wheat Grain and Condensation Prediction. Ph.D. Thesis, Jilin University, Changchun, China, 2015.
19. Zhang, R.D. Law of Occurrence and Development of Dew Condensation during Storage of Soybean and Its Influence on Quality. Master's Thesis, Henan University of Technology, Zhangzhou, China, 2021.

20. Spencer, M.R. Effect of shipping on quality of seeds, meals, fats, and oils. *J. Am. Oil Chem. Soc.* **1976**, *53*, 238–240. [CrossRef]
21. Milton, R.F.; Pawsey, R.K. Spoilage relating to the storage and transport of cereals and oil seeds. *Int. J. Food Microbiol.* **1988**, *7*, 211–217. [CrossRef]
22. Soybeans, T.G.A. Risk Factors and Loss Prevention. Available online: https://www.tis-gdv.de/tis_e/ware/oelsaat/sojabohn/sojabohn-htm/#ls (accessed on 1 July 2023).
23. Palacios-Cabrera, H.A.; Menezes, H.C.; Iamanaka, B.T.; Canepa, F.; Teixeira, A.A.; Carvalhaes, N.; Santi, D.; Leme, P.T.Z.; Yotsuyanagi, K.; Taniwaki, M.H. Effect of Temperature and Relative Humidity during Transportation on Green Coffee Bean Moisture Content and Ochratoxin A Production. *J. Food Prot.* **2007**, *70*, 164–171. [CrossRef]
24. Drzewieniecka, B.; Drzewieniecki, J.; Blatnický, M. The Influence of External Factors on Hazards in the Transport Processes of Soybean Meal. *New Trends Prod. Eng.* **2018**, *1*, 301–307. [CrossRef]
25. Uygun, Y.; Jafri, S.A.I. Controlling risks in sea transportation of cocoa beans. *Cogent Bus. Manag.* **2020**, *7*, 1778894. [CrossRef]
26. Anderson, D.; Sheard, D. *Cargo Ventilation: A Guide to Good Practice*, 2nd ed.; The North of England P&I Association: Newcastle, UK, 2020; pp. 10–19.
27. Lovstad, M. New Guidance Document for Cargo and Cargo Hold Ventilation. Available online: https://www.dnv.com/expert-story/maritime-impact (accessed on 13 August 2023).
28. Yuen, P.; Sasa, K.; Kawahara, H.; Chen, C. Statistical estimation of container condensation in marine transportation between Far East Asia and Europe. *J. Navig.* **2021**, *75*, 176–199. [CrossRef]
29. Novikova, T.; Stikhova, A.; Zhmyrko, T. Study of loose bulk cargo storage conditions and water transportation. *E3S Web Conf.* **2021**, *326*, 36. [CrossRef]
30. Ocieczek, A.; Zawadzka, D.; Kaizer, A.; Zawadzki, M. The Effects of Particular Factors Connected with Maritime Transport on Quality and Safety of Cereal As A Cargo. *Transp. Probl.* **2021**, *16*, 19–32. [CrossRef]
31. Arias, A.; Abalone, R.; Gastón, A. Mathematical modelling of momentum, heat and mass transfer in grains stored in silos. Part i: Model development and validation. *Lat. Am. Appl. Res.* **2013**, *43*, 377–384.
32. Panigrahi, S.; Singh, C.; Fielke, J.; Zare, D. Modeling of heat and mass transfer within the grain storage ecosystem using numerical methods: A review. *Dry. Technol.* **2019**, *38*, 1677–1697. [CrossRef]
33. White, N.D.G.; Sinha, R.N.; Muir, W.E. Intergranularcarbon Dioxide as an Indicatorof Biologicalactivityassociatedwith the Spoilageof Stored Wheat. *Can. Agric. Eng.* **1982**, *24*, 35–42.
34. REN, S.G.; Wei, Y.; Haoyu, W. Prediction model on temporal and spatial variation of air temperature in greenhouse and ventilation control measures based on CFD. *Transations Chin. Soc. Agric. Eng.* **2015**, *13*, 207–214.
35. Thorpe, G.R. The application of computational fluid dynamics codes to simulate heat and moisture transfer in stored grains. *J. Stored Prod. Res.* **2008**, *44*, 21–31. [CrossRef]
36. Wang, Y.C.; Yang, K.M.; Zhang, Z.T.; Qi, W.; Yang, J. Natural convection heat and moisture transfer with thermal radiation in a cavity partially filled with hygroscopic porous medium. *Dry. Technol.* **2016**, *34*, 275–286. [CrossRef]
37. World Meteorological Organization. *Guide to Meteorological Instruments and Methods of Observation*, 8th ed.; World Meteorological Organization: Geneva, Switzerland, 2018; pp. 110–111.
38. Pu, J.; Shen, C.; Zhang, C.; Liu, X. A semi-experimental method for evaluating frosting performance of air source heat pumps. *Renew. Energy* **2021**, *173*, 913–925. [CrossRef]
39. Wu, Z.; Li, X. The Use of CAE Model for Controlling Aeration in A Chinese Rough Rice Depot. *J. Chin. Cereals Oils Assoc.* **2011**, *2*, 73–78+83.
40. Sun, B.X. The Study of Temperature Field of Bulk Soybean in Ship. Master's Thesis, Dalian Maritime University, Dalian, China, 2018.
41. Ge, M.; Chen, G.; Liu, C.; Zheng, D.; Liu, W. Effect of Vertical Pressure on Temperature Field Distribution of Bulk Paddy Grain Pile. *Appl. Sci.* **2022**, *12*, 10392. [CrossRef]
42. Hristov, A. *Bulk Carrier Practice*, 2nd ed.; Nautical Institute: London, UK, 2010; pp. 76–77.
43. Sun, G.; Yang, L.; Liu, R. Thermal insulation coatings based on microporous particles from Pickering emulsion polymerization. *Prog. Org. Coat.* **2021**, *151*, 106023. [CrossRef]